Journal of Carbon Research

MDPI

Article

Investigating the Adsorption Kinetics of Dimethoate, Malathion and Chlorpyrifos on Cellulose-Derived Activated Carbons: Understanding the Influence of Physicochemical Properties

Tamara Lazarević-Pašti [1], Ana Jocić [1], Vedran Milanković [1], Tamara Tasić [1], Katarina Batalović [1], Stefan Breitenbach [2,3], Christoph Unterweger [2,*], Christian Fürst [2] and Igor A. Pašti [4]

1 VINČA Institute of Nuclear Sciences—National Institute of the Republic of Serbia, Department of Physical Chemistry, University of Belgrade, Mike Petrovica Alasa 12-14, 11000 Belgrade, Serbia; tamara@vin.bg.ac.rs (T.L.-P.); ana.jocic@vin.bg.ac.rs (A.J.); vedran.milankovic@vin.bg.ac.rs (V.M.); tamara.tasic@vin.bg.ac.rs (T.T.); kciric@vin.bg.ac.rs (K.B.)
2 Wood K plus—Kompetenzzentrum Holz GmbH, Altenberger Strasse 69, 4040 Linz, Austria; s.breitenbach@wood-kplus.at (S.B.); c.fuerst@wood-kplus.at (C.F.)
3 Institute of Chemical Technology of Inorganic Materials (TIM), Johannes Kepler University Linz, Altenberger Strasse 69, 4040 Linz, Austria
4 Faculty of Physical Chemistry, University of Belgrade, Studentski trg 12-16, 11158 Belgrade, Serbia; igor@ffh.bg.ac.rs
* Correspondence: c.unterweger@wood-kplus.at

Abstract: In light of the escalating environmental concerns regarding pesticide accumulation, it is imperative to devise efficient strategies for their removal. Among the various options, activated carbons have emerged as promising candidates for adsorptive pesticide removal due to their many advantages, such as large surface area, well-developed porosity, and cost-effectiveness. However, the intricate relationship between the properties of these materials and their performance in pesticide adsorption remains largely unexplored. This study primarily focuses on examining the adsorption kinetics of three organophosphate pesticides: dimethoate, malathion (aliphatic), and chlorpyrifos (aromatic), using a range of cellulose-based activated carbon fibers with diverse specific surface areas, pore size distributions, and elemental compositions. By employing sophisticated data analysis tools, principal component analysis, and semi-empirical quantum chemical calculations, this study uncovers the importance of these distinct properties in efficiently removing structurally diverse pesticides. The results of the adsorption experiments suggested that these processes can be described using a pseudo-second-order kinetic model, which is confirmed via multiple linear regression. The obtained data suggest that the most effective carbon material for pesticide removal should have a pore diameter of approximately 4 nm, low oxygen content, a unimodal pore size distribution, and a high presence of sp^2 domains. The insights from this research have the potential to guide the development of improved adsorbents and facilitate the rational selection of adsorbents tailored to specific pollutants based on their physicochemical properties and the pollutants' chemical structure. By shedding light on the vital connection between adsorbent properties and performance, our findings significantly advance sustainable and effective pesticide removal, thereby fostering a cleaner and healthier environment.

Keywords: organophosphate; pesticide removal; adsorption; kinetics; activated carbon; textural properties

Citation: Lazarević-Pašti, T.; Jocić, A.; Milanković, V.; Tasić, T.; Batalović, K.; Breitenbach, S.; Unterweger, C.; Fürst, C.; Pašti, I.A. Investigating the Adsorption Kinetics of Dimethoate, Malathion and Chlorpyrifos on Cellulose-Derived Activated Carbons: Understanding the Influence of Physicochemical Properties. *C* **2023**, *9*, 103. https://doi.org/10.3390/c9040103

Academic Editors: Jorge Bedia and Carolina Belver

Received: 22 September 2023
Revised: 27 October 2023
Accepted: 1 November 2023
Published: 3 November 2023

1. Introduction

Organophosphates (OPs) represent a widely used class of pesticides, posing a significant global threat to both the environment and human health [1–3]. Their toxicity towards animals stems from their inhibition of acetylcholinesterase (AChE), a critical enzyme in

the nervous system [4,5]. To combat this pressing issue, several methods have been employed for pesticide removal from the environment, including adsorption, degradation, and microbiological treatment [6]. Among these approaches, adsorption stands out as the most widely utilized due to its effectiveness, affordability, environmental friendliness, and robustness [7,8]. Activated carbon, a highly effective adsorbent widely used in diverse applications, is often used for this purpose.

Carbon materials form a diverse and extensive group, exhibiting a wide range of textures, structures, and unique characteristics. Due to their exceptional combination of physical and chemical properties and their biocompatibility and versatility, these materials find numerous applications across various fields of science and engineering. There are unique challenges to be faced when considering activated carbon fibers compared to conventional activated carbon powders. While activated carbon fibers offer advantages like improved mechanical strength and filtration due to their fibrous structure, they may exhibit a reduced adsorption capacity, increased processing complexity, limited application range, and regeneration difficulties. The choice between these forms hinges on the specific requirements of the application and the trade-offs between the adsorption capacity, cost, and regenerability [9]. Notably, the popularity of carbon materials has witnessed a remarkable surge with the advent of biomass-based carbon materials, due to their abundance of versatile and highly porous structures and their cost-effectiveness [10,11]. Moreover, using waste biomass in carbon material production addresses increasingly critical aspects of sustainability and circularity, further enhancing their appeal.

Several factors influence the adsorption of organic compounds onto carbon materials. Most important are the properties of the adsorbent [12–14], the characteristics of the adsorbate [12,14], and the conditions of the solution [12–14].

Regarding the adsorbent's characteristics, key factors include the structure and size of pores, the chemical surface area, specific surface area, pore volume, mesopore, micropore, and nanopore volume, the presence of surface functional groups, and the zero charge point (pH_{pzc}) [12,14,15]. As the pore size decreases, the contact between the adsorbate and the adsorbent surface increases, thus creating more prominent interactions between the adsorbate and adsorbent and increasing the energetics of the interaction [16]. The adsorption strength also rises when the adsorption potentials between opposite pore walls overlap, which occurs when the micropore width is less than approximately twice the adsorbate diameter, as observed in gas (N_2) adsorption [17,18], methyl tertiary-butyl ether, and trichloroethene [19]. Moreover, the adsorption capacity generally increases with a higher specific surface area due to the availability of more adsorption sites [14], although this is not universally applicable. The surface chemistry of activated carbon depends on the content of heteroatoms, primarily oxygen complexes on the surface, which determine the surface charge, hydrophobicity, and electron density [13].

Crucial characteristics of the adsorbate that significantly impact the adsorption process include pKa, functional groups, polarity, molecular weight and size [12], solubility, and the nature of the substituent [13]. The size of the molecules governs the accessibility to carbon pores, while solubility influences hydrophobic interactions. The pKa value plays a critical role in the dissociation of adsorption, particularly in the case of electrolytes. Additionally, aromatic ring substituents, much like graphene layer substituents, can modulate the electron distribution, affecting dispersion interactions between the adsorbate's aromatic ring and the graphene layers within the adsorbent [13]. For instance, Haghseresht et al. [12] demonstrated that hydrophilic activated carbons primarily exhibit dominant adsorption forces through dipolar interactions when solutes are in their molecular form. Conversely, dispersive forces were found to be predominant for basic hydrophobic carbons and the same type of adsorbates. However, dispersive forces were deemed operative when the adsorbates were in their ionic forms, irrespective of the carbon surface type. In this study, p-cresol, p-nitrophenol, benzoic acid, nitrobenzene, and salicylic acid were used as probing adsorbates to investigate the adsorption properties of carbons.

The adsorption process is also influenced by solution conditions such as pH, ionic strength, and temperature [12–14]. Notably, the pH of the solution plays a critical role in determining the surface charge of carbon materials and the dissociation or protonation of electrolytes [13]. When the pH of the solution surpasses the carbon material's zero charge pH, the surface acquires a negative charge and becomes capable of attracting cations from the solution. Conversely, when the pH falls below the carbon material's zero charge pH, the surface turns positive, attracting anions [13,15,20,21]. A higher pH_{pzc} value results in a higher adsorption rate in basic solutions. Similarly, in acidic solutions, a lower pH_{pzc} results in a higher adsorption rate [15,21]. These findings have been demonstrated for reactive dyes, including methylene blue [21]. Additionally, the solution's pH controls the dissociation or ionization of electrolytes through their respective pKa values, where acidic electrolytes dissociate at a pH > pKa [13].

In the aqueous phase, a variety of interactions, including van der Waals, induced-dipole, dipole–dipole, and donor–acceptor hydrogen bonding forces, play crucial roles in binding and accumulating chemical compounds on carbonaceous adsorbents [14]. Among these interactions, hydrogen and π–π bonds, covalent and electrostatic interactions, as well as the hydrophobic effect, contribute significantly to the adsorption process [14,22,23].

Ionic strength is another pivotal factor influencing electrostatic interactions. By increasing the solution's ionic strength, attractive and repulsive interactions can be reduced due to the screening effect of the surface charge produced by the added salt. As a result, increasing the ionic strength leads to enhanced adsorption when electrostatic interactions between the surface and adsorbate are repulsive or when the surface concentration is sufficiently high. Conversely, increasing ionic strength will reduce adsorption when electrostatic interactions are attractive or when the surface concentration is relatively low. Concerning the impact of temperature on the adsorption process, a decrease in adsorption temperature is generally expected to lead to an increased intake of organic molecules since adsorption is a spontaneous process. However, some instances demonstrate an increase in the adsorbed amount with temperature [13], which is not typical for adsorption. Primarily, adsorption is an exothermic process, meaning that the adsorption capacity decreases with the increase in temperature, but in some cases, high temperature can be more beneficial for the adsorption of molecules on the surface of the adsorbent. This can be explained by the fact that when the temperature increases, an enhancement in the diffusion rate of the molecules adsorbed on the adsorbent surface through the external boundary layer and into the internal pores can occur, leading to a higher adsorption rate. Also, temperature can affect the adsorbent and its adsorption sites and activity, e.g., an increase in the available pores for adsorption might occur due to deformation of the adsorbent with increasing temperature.

While numerous materials have been investigated as adsorbents, a comprehensive understanding of the critical material properties that define adsorption performance remains elusive. This complexity arises from the interplay of multiple parameters influencing the adsorption process. In this paper, we present a systematic analysis using a well-characterized series of activated carbon fibers to explore the impact of their properties on the kinetics of chlorpyrifos, dimethoate, and malathion adsorption from aqueous solutions. Specifically, we correlate adsorbent properties such as pore volume integrated up to a given pore diameter, total pore volume, surface area, and elemental content with the kinetics of pesticide adsorption onto the investigated materials. Multiple linear regression analysis is employed to accomplish this task, aided by theoretical calculations. By combining empirical data with theoretical insights, we propose an optimal adsorbent with an ideal combination of pore diameter, sp^2 domains, and heteroatom concentration for efficient chlorpyrifos, dimethoate, and malathion adsorption. This innovative approach provides valuable information for the rational design of materials with immense potential for applications in environmental protection. Through this study, we aim to contribute significantly to the understanding of the critical factors influencing adsorption performance, paving the way for developing highly effective and tailored materials for tackling pesticide contamination in aqueous environments.

2. Materials and Methods

2.1. Activated Carbon Fiber Preparation

The preparation of activated carbon fibers (ACF) is described in [24] and reproduced here for completeness. Viscose fibers 1.7 dtex, 38 mm (Lenzing AG, Lenzing, Austria), were impregnated with diammonium hydrogen phosphate (DAHP) solutions of different concentrations (0.0–75.7 mmol dm^{-3}, corresponding to 0.00–10.00 wt.% DAHP) for 15 min. After a 24 h drying period, carbonization was conducted at 850 °C for 20 min under a nitrogen atmosphere, with a heating rate of 1.0 °C min^{-1}. The carbonized fibers were then activated at 870 °C for 165 min with CO_2 flow (80 dm^3 h^{-1}). No additional washing was needed due to pure precursor fibers and non-altering impregnation agents [25–27]. The samples were labeled as DAHP-X, where X represents the concentration of DAHP used in the impregnation step.

2.2. Characterization of Materials

The ACF samples' morphology and elemental composition were investigated using a scanning electron microscope (PhenomProX, Thermo Fisher Scientific, Waltham, MA, USA) equipped with energy-dispersive X-ray spectroscopy (EDX). The textural properties and specific surface area of materials were studied via N_2 isothermal adsorption (−196.15 °C). For this purpose, a gas sorption system was used (AutosorbiQ, Quantachrome Instruments, Graz, Austria). The specific surface area and derived pore size distribution (PSD) were calculated using the Brunauer–Emmett–Teller (BET) method and the non-local density functional theory (NLDFT), respectively [28–30].

2.3. Pesticide Adsorption Measurements

Batch adsorption experiments were performed by dispersing the materials in double distilled water and adding the required pesticide stock solution (Pestanal, Sigma Aldrich, Søborg, Denmark) to achieve the desired concentrations of adsorbent and pesticide. The mixtures were then placed on an Orbital Shaker-Incubator at 25 °C for specific periods of time. After centrifugation and filtration, ultra performance liquid chromatography (UPLC) was used to determine the concentration of organophosphates (C_{eq}). Control experiments were conducted without materials to confirm no pesticide degradation. The pH of the dispersions remained consistent, indicating that differences in pesticide removal kinetics were solely due to adsorption on the materials. UPLC measurements were performed using an ACQUITY UPLC system (Waters, Milford, MA, USA) with a tunable UV detector and an ACQUITY UPLC™ BEH C18 column (1.7 µm, 100 mm × 2.1 mm, Waters, Milford, MA, USA) under isocratic conditions with acetonitrile and water as the mobile phase (see ref. [29] for details).

2.4. Principal Component Analysis

The principal component analysis (PCA) was conducted using the built-in functions provided by Scikit-learn. To ensure effective statistical analysis, the input variables were scaled using the StandardScaler function, accommodating various levels and ranges of the considered data.

2.5. Semi-Empirical Quantum Chemical Calculations

Semi-empirical calculations were performed using the MOPAC2016 code [31] with the PM7 method [32]. A model of (7,7) SWCNT was constructed with 112 atoms to obtain the deformation energies of chlorpyrifos. Then, the chlorpyrifos molecule was placed into the tube, and full structural relaxation was carried out. After the relaxation, the system was split into nanotube and chlorpyrifos parts, and their molecular energies were calculated in a self-consistent cycle. Deformation energies were obtained by comparing the energy of fully relaxed chlorpyrifos/nanotube with the energy of chlorpyrifos/nanotubes with the mathematical result corresponding to the chlorpyrifos inserted into the nanotube.

3. Results

3.1. Materials Properties

The materials studied in this work have been partially characterized and investigated, with respect to the thermodynamic properties' influence on adsorption capacities, before [24,29]. One of the main conclusions was that the specific surface area does not play a dominant role in determining the adsorption capacity but rather pore volume and carbon and oxygen content do. However, the studied materials are micro- and mesoporous with different pore size distributions (Figure 1). Thus, it is still unclear which portion of the total pore volume is responsible for the overall uptake of pollutants, and particularly the kinetics of this process. This work aims to correlate the kinetics of pesticide adsorption to the adsorbents' physicochemical properties. Detailed analysis of the pore size distribution and elemental content of the materials are provided in Table 1. From the data presented, it is clear that the chemical composition of the adsorbents was influenced by the loading of DAHP during the impregnation process. Utilizing EDX, we observed a consistent rise in the phosphorus (P) content in the materials, while the levels of carbon (C) and oxygen (O) exhibited fluctuations but no obvious trend. Notably, the initial phosphorus-containing sample in the series exhibited a significant decrease in specific surface area (S_{tot}) when compared to the material produced without DAHP impregnation. Furthermore, as the concentration of DAHP increased, both the S_{tot} and total volume (V_{tot}) increased. Additionally, the increase in phosphorus content led to a gradual increase in pore sizes.

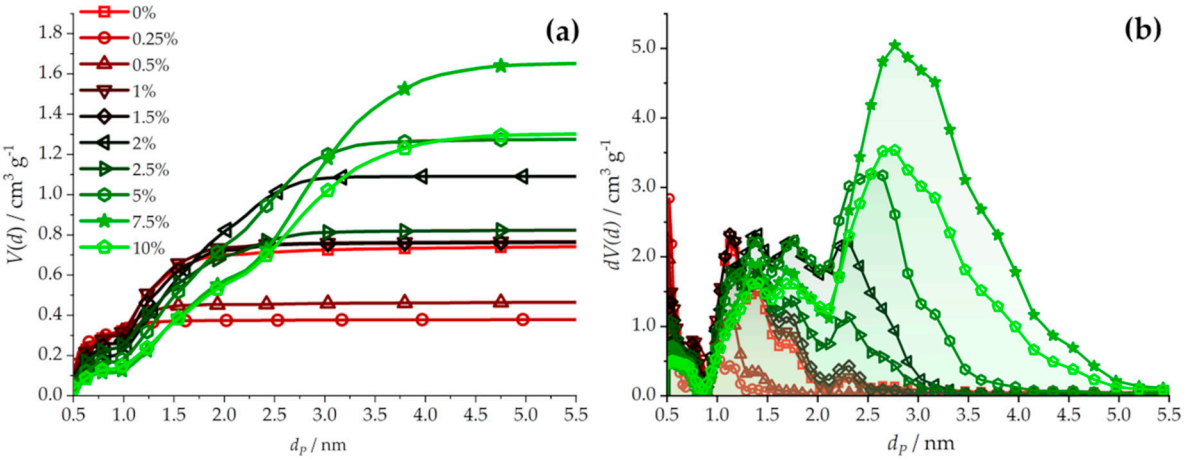

Figure 1. (**a**) Integral pore volumes up to a given pore diameter function; (**b**) common pore size distribution curves for studied adsorbents. The notation of samples is DAHP-X, where X is given in the figure legend.

Integral (Figure 1a) and differential pore volume (Figure 1b) distributions reveal that pore volumes increase with the amount of DAHP used, while pore sizes also increase. Table 1 shows the same trend. For example, the volume of pores with a diameter below 1 nm decreases along the series, while the total pore volume increases. The exception is the first sample in the series, DAHP-0, which has a higher V_{tot} than the samples DAHP-0.25 and DAHP-0.50, and also a higher specific surface area. We note that in these experiments, the ultramicropores were not able to be measured, but, based on the results presented later on, it is not likely that this fraction of pores can significantly contribute to the adsorption process.

As explained previously [24,29], these materials are particularly suitable for testing different hypotheses about the adsorption process. All these materials have been derived from the same precursor and have identical morphology (Figure 2). During the carbonization and activation steps, all samples kept their initially identical morphology, with the surface texture of the precursor being retained and the fiber diameter showing a similar

shrinkage of approx. 25% for all samples. For this reason, the effects of the morphology on the rate of the adsorption processes can be safely excluded.

Table 1. Adsorbents' properties–pore volume integrated up to a given pore diameter, total pore volume (integrated up to pore diameter of 35 nm), surface area, and elemental content, determined using energy dispersive X-ray spectroscopy. The notation of samples is DAHP-X, where X represents the concentration of DAHP in wt.% used for the impregnation step.

X =		**0.00%**	**0.25%**	**0.50%**	**1.00%**	**1.50%**	**2.00%**	**2.50%**	**5.00%**	**7.50%**	**10%**
Pores up to (volume/cm^3 g^{-1})	1 nm	0.348	0.335	0.339	0.343	0.297	0.271	0.274	0.198	0.137	0.160
	2 nm	0.702	0.375	0.454	0.738	0.723	0.857	0.696	0.754	0.580	0.559
	3 nm	0.725	0.377	0.459	0.759	0.756	1.086	0.813	1.200	1.180	1.021
	4 nm	0.734	0.378	0.462	0.763	0.760	1.091	0.819	1.267	1.568	1.254
V_{tot} */cm^3 g^{-1}		0.757	0.383	0.472	0.774	0.770	1.094	0.833	1.291	1.681	1.322
S_{tot} **/m^2 g^{-1}		1932	1016	1250	2037	2002	2556	2018	2718	2763	2718
Elemental Content **	C/at.%	92.4 ± 2.1	91.6 ± 3.5	93.6 ± 2.3	87.9 ± 1.3	93.9 ± 1.9	91.3 ± 2.0	87.9 ± 2.0	85.6 ± 2.5	82.2 ± 2.2	77.8 ± 5.0
	O/at.%	7.6 ± 2.0	8.4 ± 3.5	6.2 ± 2.2	12 ± 1.3	5.9 ± 1.9	7.7 ± 2.3	11.4 ± 2.2	13.1 ± 2.7	16.1 ± 2.3	19.7 ± 5.3
	P/at.%	0	0.02 ± 0.02	0.18 ± 0.10	0.11 ± 0.04	0.28 ± 0.07	0.91 ± 0.29	0.65 ± 0.30	1.32 ± 0.34	1.78 ± 0.13	1.9 ± 0.64

* Integrated up to 35 nm; ** Reference [24].

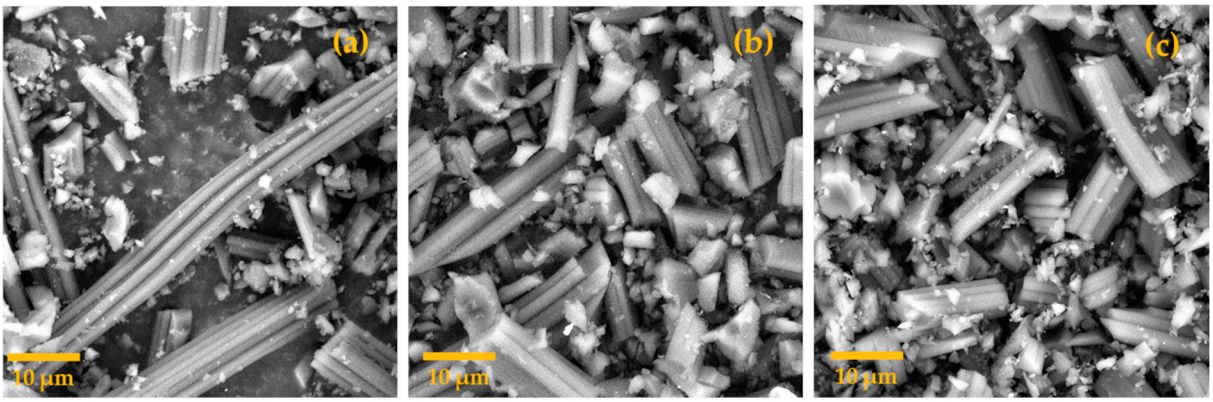

Figure 2. SEM images of the (**a**) DAHP-0.00% sample; (**b**) DAHP-5.00% sample; and (**c**) DAHP-10.00% sample. Magnification ×5000, scale bar 10 µm, the field of view 53.3 µm.

Moreover, all the samples have undergone the same milling procedure, so the effects particle sizes on the adsorption performance can also be excluded. Additionally, due to the same carbonization and activation temperatures, the Raman spectra of all the samples were identical [24]. Thus, the effects of the disorder degree can also be excluded. That leaves pore size distribution and elemental content (Table 1), effectively tuned by the amount of impregnating agent, DAHP, as the decisive properties that affect the adsorption kinetics. Due to the careful synthesis design, the parametric space in which the adsorption process can be investigated is significantly reduced, allowing for the derivation of more straightforward conclusions about the effects of adsorbent properties on the adsorption kinetics.

3.2. Performance of the Materials

In the forthcoming sections, the adsorption data for chlorpyrifos, dimethoate, and malathion are analyzed. First, the adsorption was analyzed for up to 60 min, and the concentration of the pesticide remaining in the solution at a given moment was evaluated using UPLC analysis (Section 2, see Figures S1–S3, Supplementary Materials). Then, the amount of adsorbed pesticide in a given moment (q_t) was fitted into the kinetic equations, assuming kinetics obeying pseudo-first- (Equation (1)) and pseudo-second-order (Equation (2)):

$$\ln(q_e - q_t) = \ln(q_e) - k_1 t \quad (1)$$

And

$$\frac{t}{q_t} = \frac{1}{k_2 q_e^2} + \frac{1}{q_e} t \quad (2)$$

where q_e is the equilibrium adsorption capacity, while k_1 and k_2 are the pseudo-first and pseudo-second rate order constants. The obtained rate order constants for chlorpyrifos, dimethoate, and malathion are presented in Tables 2–4.

Table 2. Rate constants for chlorpyrifos removal. The notation of samples is DAHP-X, where X represents the concentration of DAHP in wt.% used for the impregnation step. The chlorpyrifos concentration was 1×10^{-4} mol dm^{-3}, while the adsorbents' concentration was 0.1 mg mL^{-1} in each case.

X =	0.00%	0.25%	0.50%	1.00%	1.50%	2.00%	2.50%	5.00%	7.50%	10%
					Pseudo-first order					
k_1/min^{-1}	0.054	0.034	0.0596	0.049	0.048	0.048	0.053	0.047	0.055	0.045
Δk_1/min^{-1}	0.022	0.012	0.0048	0.015	0.014	0.018	0.019	0.015	0.025	0.023
R^2	0.7206	0.75	0.98728	0.81	0.84	0.75	0.78	0.82	0.66	0.58
					Pseudo-second order					
k_2/g mg^{-1} min^{-1}	0.0053	0.0086	0.0032	0.0028	0.0030	0.0052	0.0067	0.0045	0.0134	0.0085
Δk_2/g mg^{-1} min^{-1}	7×10^{-4}	8×10^{-4}	2×10^{-4}	8×10^{-4}	7×10^{-4}	1×10^{-4}	1×10^{-4}	1×10^{-4}	2×10^{-4}	3×10^{-4}
R^2	0.9995	0.98	0.99996	0.998	0.998	0.9991	0.9995	0.998	0.9996	0.998

Table 3. Rate constants for dimethoate removal. The notation of samples is DAHP-X, where X represents the concentration of DAHP in wt.% used for the impregnation step. The dimethoate concentration was 1×10^{-4} mol dm^{-3}, while the adsorbents' concentration was 0.1 mg mL^{-1} in each case.

X =	0.00%	0.25%	0.50%	1.00%	1.50%	2.00%	2.50%	5.00%	7.50%	10%
					Pseudo-first order					
k_1/min^{-1}	0.204	0.044	0.074	0.039	0.070	0.088	0.053	0.0368	0.055	0.142
Δk_1/min^{-1}	0.072	0.021	0.025	0.016	0.018	0.012	0.013	0.0026	0.011	0.020
R^2	0.64	0.53	0.65	0.72	0.78	0.95	0.85	0.98	0.88	0.94
					Pseudo-second order					
k_2/g mg^{-1} min^{-1}	0.281	0.048	0.016	0.017	0.0343	0.0064	0.040	0.0069	0.030	0.092
Δk_2/g mg^{-1} min^{-1}	6×10^{-3}	2×10^{-3}	1×10^{-3}	2×10^{-3}	6×10^{-4}	5×10^{-4}	3×10^{-3}	6×10^{-4}	3×10^{-3}	2×10^{-3}
R^2	0.99997	0.98	0.998	0.98	0.998	0.992	0.997	0.94	0.998	0.9998

Table 4. Rate constants for malathion removal. The notation of samples is DAHP-X, where X represents the concentration of DAHP in wt.% used for the impregnation step. For the adsorption measurements, the concentration of malathion was 1×10^{-4} mol dm^{-3}, while the adsorbents' concentration was 0.1 mg mL^{-1} in each case.

X =	0.00%	0.25%	0.50%	1.00%	1.50%	2.00%	2.50%	5.00%	7.50%	10%
					Pseudo-first order					
k_1/min^{-1}	0.055	0.49	0.70	0.402	0.234	0.214	0.149	0.143	0.064	0.223
Δk_1/min^{-1}	0.012	0.20	0.27	0.087	0.025	0.073	0.016	0.033	0.026	0.013
R^2	0.86	0.61	0.66	0.87	0.97	0.72	0.98	0.85	0.64	0.99
					Pseudo-second order					
k_2/g mg^{-1} min^{-1}	0.0075	0.0214	0.0085	0.0608	0.1002	0.0754	0.0166	0.0070	0.0634	0.0097
Δk_2/g mg^{-1} min^{-1}	2×10^{-4}	6×10^{-4}	5×10^{-4}	3×10^{-4}	7×10^{-4}	7×10^{-4}	3×10^{-4}	7×10^{-4}	4×10^{-4}	2×10^{-4}
R^2	0.998	0.996	0.98	0.9998	0.99999	0.99998	0.9997	0.9996	0.9998	0.998

From the value of k_1, the adsorption half-time ($t_{1/2}$) can be calculated as

$$t_{1/2} = \frac{\ln 2}{k_1} \quad (3)$$

which gives the time at which half of the pesticide adsorption capacity is taken up by the adsorbent.

3.2.1. Chlorpyrifos Removal

The rate constants for chlorpyrifos removal are given in Table 2. It can be seen that the rate constants for pseudo-first-order reaction kinetics are determined with large uncertainties. In contrast, rate constants are determined more reliably for the pseudo-second-order kinetics. This is partially contributed to by the fact that a linearized form of the equation for the second-order kinetics was used. While linearized forms are easier to handle, they artificially increase the correlation coefficient [33]. However, for this investigation, the overall trends and their connection with the materials' properties are of interest rather than determining the adsorption rate constants with high accuracy. Apparently, there is no association between the chlorpyrifos removal constants and the overall trends in the materials' properties (Table 1)—an overall increase in total pore volume and an increase in O and P atomic content. Although the reliability of the pseudo-first-order constants is not high, it is possible to conclude that the half-times for chlorpyrifos adsorption are of the order of 10 min. This result aligns well with previous adsorption kinetics studies of different pesticides on carbon materials [34–37]. Minute ranges of chlorpyrifos adsorption half-times were reported for gamma radiation-modified activated carbon [38], while graphitic carbon nitride (g-C_3N_4)-incorporated chitosan showed chlorpyrifos adsorption kinetics very similar to the presented ACFs [39]. Nevertheless, the half-times obtained here were much higher compared to, for example, the one found for chlorpyrifos removal by an NU-1000 metal–organic framework, which was only 0.43 min [40].

3.2.2. Dimethoate and Malathion Removal

In contrast to chlorpyrifos, which possesses an aromatic ring in its structure, dimethoate and malathion are aliphatic molecules. Nevertheless, the same general observations that are made for chlorpyrifos hold for dimethoate and malathion adsorption kinetics, as well. There are no apparent trends, and k_2 is determined with higher reliability than k_1. The half-times for dimethoate adsorption are in the range of 3.4–17.8 min. For malathion, the range is 1–12.6 min. Similarly to chlorpyrifos, the estimated half-times for dimethoate adsorption on studied ACFs are in the same range or lower, compared to those found in the literature or calculated based on reported k_1, as with the case of KOH-modified *Thevetia peruviana* shell-activated carbon [41]. The studied ACFs are very efficient adsorbents for malathion removal and also possess better adsorption kinetics than some other carbons, like waste-derived activated carbons [26].

4. Discussion

Multiple linear regression analysis was used to investigate the impact of material properties on the adsorbents' performances. It is a relatively simple tool but can reveal some hidden links between dependent and independent variables, which can only be easily understood with the help of statistical tools. In short, it is assumed that the rate constants k_1 or k_2 can be presented as a linear combination of the properties (x_i) given in Table 1 with corresponding coefficients (A_i) as

$$k = \sum_i A_i x_i \quad (4)$$

Counter i is 1–4 for pore volumes up to 1, 2, 3, and 4 nm, respectively, 5 for total pore volume, and 6–8 for C, O, and P atomic content. The results of the linear regression analysis are given in Figure 3. Before the analysis, k_1 and k_2 were multiplied by 100. At the same time, the C and O contents were divided by 100 and 10, respectively, to scale all the quantities used in the analysis to similar orders of magnitude.

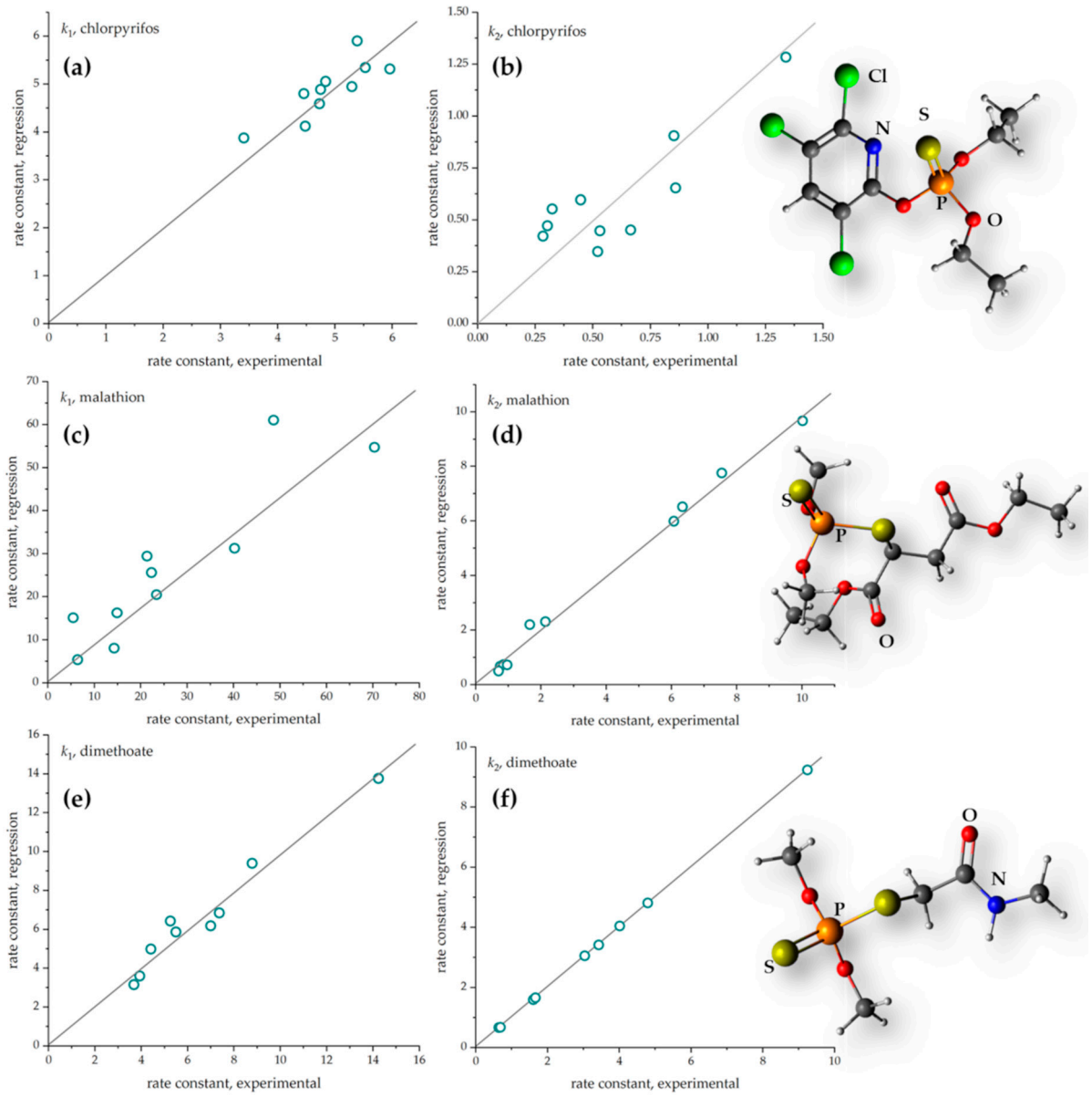

Figure 3. The results of multiple linear regression analysis (**a**) k_1 for chlorpyrifos, (**b**) k_2 for chlorpyrifos, (**c**) k_1 for dimethoate, (**d**) k_2 for dimethoate, (**e**) k_1 for malathion, and (**f**) k_2 for malathion.

To analyze the impact of different materials' properties, one should also consider the properties of the adsorbates. Malathion, dimethoate, and chlorpyrifos are of similar sizes, around 1 nm along the longest axis of a molecule, but with some differences in branching. Also, chlorpyrifos has an aromatic ring [29]. Thus, the accommodation of all three molecules into the pore structure of studied adsorbents should start from pores with a diameter above 1 nm. However, it could be even a little larger as both adsorbent and adsorbate are solvated, which effectively reduces the pore diameter while increasing the dimensions of the adsorbate.

Now, if the results of the linear regression analysis are considered (Figure 3 and Table A1), it is evident that generally good predictions for adsorption rate constants are obtained. This is particularly true for pseudo-second-order kinetics in the cases of dimethoate and malathion. In both cases, three independent variables stand out. First, the model is susceptible to the cumulative pore volumes for pores with diameters up to 2 nm and 4 nm, which positively correlate to the rate constants. Second, the carbon content (Table 1) also seems to be a determinant of fast adsorption kinetics. As discussed before [24,29],

there are indications that for the studied materials, physisorption is operative. Thus, a positive correlation of carbon content with adsorption rate constants can be understood through the reduced number of highly solvated domains. However, O atomic content also positively correlates with the adsorption rate constants (much more so for malathion than dimethoate). It can be due to dipole–dipole [42] and electrostatic interactions, which can positively affect the adsorption rates in accordance with the charges of the adsorbate molecules and adsorbent. If their charges are opposite, the adsorption will be promoted and the adsorption rates will be enhanced [43,44]. If some highly oxidized domains are present at the pore openings, they might block the entrance of pesticides into the pores, reducing the adsorption capacity and impeding the adsorption process rate.

To analyze the correlation between the various input features given in Table 1 and the pseudo-second-order adsorption rate constants of three studied pesticides, Pearson correlation coefficients are calculated to depict the degree of correlation between the variables (Figure 4).

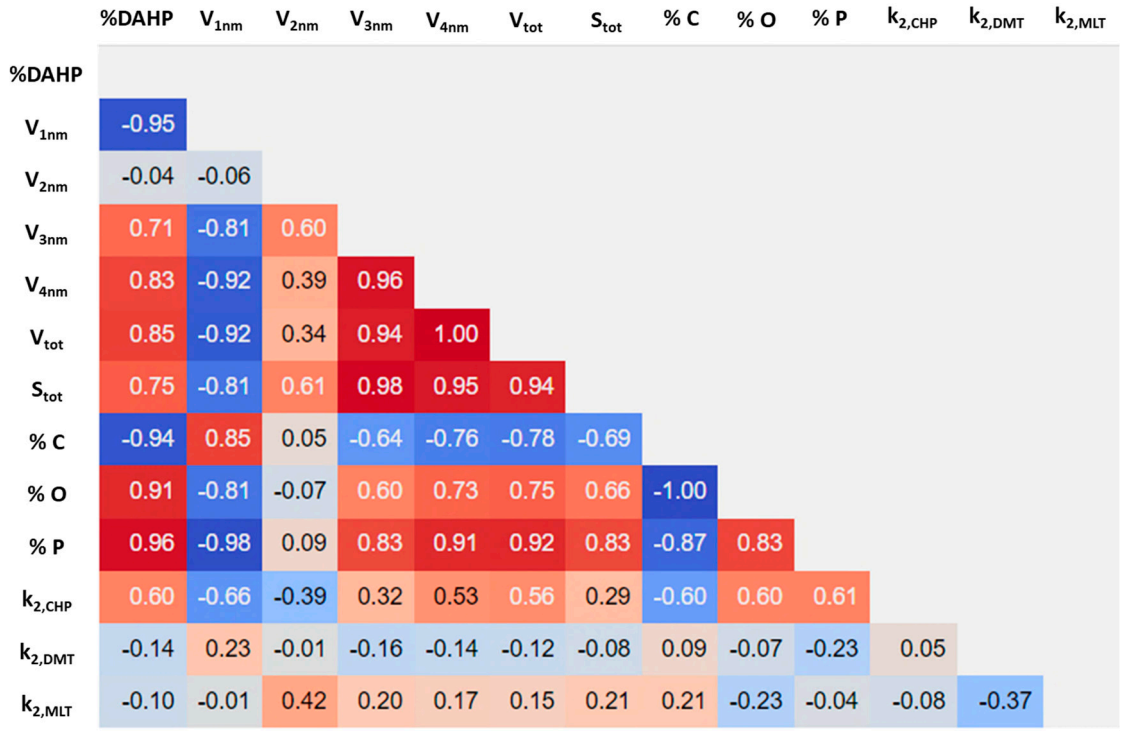

Figure 4. Heat map of the Pearson correlation matrix coefficients between various features, including material-related properties (Table 1) and pseudo-second-order rate constants for pesticide adsorption (Tables 2–4). The intensity of red indicates the strength of a positive correlation, while the intensity of blue indicates the strength of a negative correlation. Abbreviations used: %DAHP—percentage (X) of DAHP in the impregnation step, V_{Ynm}—pore volume up to the width of Y nm (Y = 1, . . ., 4), elemental content in at.%, and k_2—pseudo-second-order adsorption rate constant of malathion (MLT), dimethoate (DMT), and chlorpyrifos (CPF).

Regarding the correlation of the studied material-related properties, we find that all of them, except the V_{2nm}, are strongly correlated and significantly correlated with the pseudo-second-order adsorption rate constant for chlorpyrifos ($k_{2,CHP}$). However, we do not find any significant correlation to the other two studied pesticides with these features. Importantly, %DAHP is negatively correlated to V_{1nm}, which might be explained by the increasing activation rate at higher DAHP content sizes of the molecule. The pore development in correlation with the impregnation ratio and activation yield has been discussed in detail previously [45]. A moderate positive correlation between the used DAHP percentage and $k_{2,CHP}$ allows for the training of linear regression models with this

feature as the only input. It depicts the important aspects of this pretreatment to the rate of chlorpyrifos removal. Based on the Pearson correlation coefficients $\geq$0.6, we can relate the success of DAHP as a modifier in this case to the decrease in V_{1nm} and changes in the sample's elemental composition. The lack of significant correlation of any input feature to $k_{2,DMT}$ and $k_{2,MLT}$ might also be due to the low capacity of pesticide removal in these cases.

It is interesting to observe the role of the cumulative pore volumes based on the multiple linear regression models. Namely, there are indications that the first limit corresponds to the entrance of individual molecules (including their solvation shells) into the pores in such a way that one molecule interacts with two opposite sides of the pore interior along the pore size diameter (Figure 5a). The second situation (4 nm) corresponds to the case where the adsorbate molecule interacts with one side of the pore interior, but the pore diameter is large enough to accommodate two adsorbate molecules along the pore size diameter (Figure 5b).

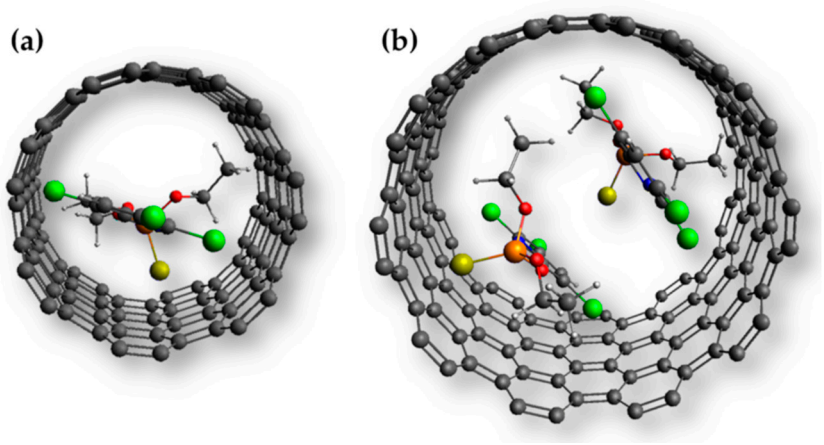

Figure 5. Schematic representation of the accommodation of chlorpyrifos molecules into pores of different diameters: (**a**) when the pore diameter allows for the entrance of only one molecule, (**b**) when the pore diameter is sufficient to place two chlorpyrifos molecules in the pore. Any pores with diameters between the hypothetical cases of (**a**,**b**) can only accommodate one molecule along the pore diameter.

The diffusion of organophosphate molecules into the pore system of adsorbents is likely to be spontaneous and without the significant deformation of pesticide molecules, which would produce a large energy penalty during this process. To check for this assumption, semi-empirical quantum chemical calculations on the chlorpyrifos inserted into the interior of a (7,7) single-walled carbon nanotube (SWCNT) were performed, imitating the interior of a pore of the studied ACFs. Such a SWCNT has a diameter of 9.5 Å (if the length is infinite). For the finite-sized SWCNT studied in this case, the aliphatic part of the chlorpyrifos molecule is "expelled" from the tube (Figure 6a). At the same time, both chlorpyrifos and the nanotube undergo significant deformation (Figure 6b). The deformation energy of the chlorpyrifos molecule is 33 kJ mol^{-1}, while for SWCNT, it amounts to 710 kJ mol^{-1} (please note that this energy relates to 1 mol of the finite-size SWCNTs used in this study). Even without a solvent shell, the entrance of chlorpyrifos into pores smaller than 1 nm is unlikely. Moreover, one should acknowledge that the studied pesticides do not have molecules which are perfect spheres. For example, in the case of chlorpyrifos, presented here, the longer axis of the molecule is approx. 1.08 nm, while the molecule dimension perpendicular to this axis is approx. 0.85 nm. Moreover, polar parts of the molecules become more heavily solvated compared to non-polar ones, which additionally complicates the situation. A particular orientation of the molecules is absolutely necessary for them to enter the pores, but at this point it is unclear whether molecular reorientation and proper placement at the pore openings can be the rate-determining step for adsorption in the pores. An additional point relates to the surface functional groups at the pore openings, which can affect molecular reorientation and/or partial desolvation during adsorption

in the pores. Finally, it should be noted that the rate constants obtained here generally do not correlate with the adsorption capacities [24,27]. Hence, one should consider the properties that determine the materials' adsorption capacities and fast adsorption kinetics under the desired conditions to design proper adsorbents for different pesticides.

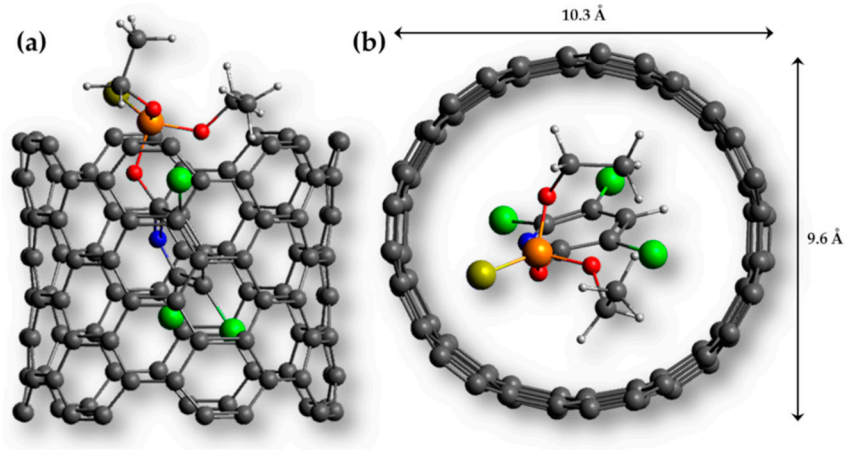

Figure 6. Entrance of a chlorpyrifos molecule into the SWCNT: (**a**) side view, (**b**) a view along the SWCNT (pore) axis; the deformation is visible as the SWCNT deviates from the circular shape.

5. Conclusions

In this study, the kinetics of chlorpyrifos, dimethoate, and malathion adsorption on a series of activated carbon fibers with diverse pore structures and chemical compositions were analyzed. The adsorption data were processed to obtain pseudo-first- and pseudo-second-order rate constants. No particular trend was found in connection with the studied materials' properties alone (integral pore volumes, the content of C, O, P). However, employing multiple linear regression allowed for the establishment of connections between the materials' properties and the adsorption kinetics. Specifically, for dimethoate and malathion, the regression analysis provided reliable predictions for the pseudo-second-order kinetics rate constants, while for chlorpyrifos, the performance of the regression model was lower. Among the considered material properties, cumulative pore volumes up to 2 nm and 4 nm and the carbon content showed strong positive correlations with the rate constants. This observation suggests an interplay between the sizes of pesticide molecules and pore diameters, enabling the accommodation of one or two pesticide molecules within the pore diameter. Theoretical calculations further indicated that, in the absence of a solvent, the penetration of pesticide molecules into pores with a diameter below 1 nm is unlikely without significant deformation of the molecule (and the pore). Such a process would require a considerable energy input, making it thermodynamically unfavorable. To optimize the design or selection of adsorbents for particular applications, it is essential to strike a balance between the properties governing the adsorption capacities and kinetics, as these two aspects are not directly correlated. The ideal adsorbent for the pesticides under study would be a mesoporous carbon material featuring a pore diameter of around 4 nm, along with a unimodal pore size distribution. Additionally, it should possess a relatively low concentration of oxygen (and potentially other heteroatoms) while maintaining a significant presence of sp^2 domains. The findings in this study provide valuable insights into the critical factors influencing the adsorption kinetics for these pesticides, which can contribute to the development and optimization of efficient adsorbents in various environmental and industrial applications.

Supplementary Materials: The following supporting information can be downloaded at https://www.mdpi.com/article/10.3390/c9040103/s1, Figure S1: PDA signal of malathion (5×10^{-4} mol dm^{-3}) with chromatogram and the UV-Vis spectrum at the selected retention time. Figure S2: PDA signal of dimethoate (5×10^{-4} mol dm^{-3}) with chromatogram and the UV-Vis spectrum at the selected

retention time.; Figure S3: PDA signal of chlorpyrifos (5×10^{-4} mol dm^{-3}) with chromatogram and the UV-Vis spectrum at the selected retention time.

Author Contributions: Conceptualization, I.A.P. and T.L.-P.; methodology, I.A.P., S.B., C.U., C.F., and T.L.-P.; software, I.A.P.; formal analysis, A.J., V.M., T.T. and K.B.; investigation, A.J., V.M., T.T., K.B., S.B. and C.U.; resources, I.A.P., C.F. and T.L.-P.; writing—original draft preparation, I.A.P., V.M., T.T., K.B., A.J. and T.L.-P.; writing—review and editing, I.A.P., S.B., C.U., C.F. and T.L.-P.; All authors have read and agreed to the published version of the manuscript.

Funding: S.B.: C.U., and C.F. gratefully acknowledge financial support through the COMET Programme (Competence Centers for Excellent Technologies) operated by the Austrian Research Promotion Agency (FFG) and funded by the Austrian ministries BMK, BMAW, and the federal states of Upper Austria, Lower Austria, and Carinthia. T.L.P., A.J. V.M., K.B., and T.T. acknowledge the support provided by the Serbian Ministry of Education, Science and Technological Development (Contract number: 451-03-47/2023-01/200017). I.A.P. acknowledges the support provided by the Serbian Ministry of Education, Science, and Technological Development (Contract number: 451-03-47/2023-01/200146).

Data Availability Statement: Data are available upon reasonable request.

Conflicts of Interest: The authors declare no conflict of interest.

Appendix A

Table A1. Multiple linear regression parameters. See Section 4 for the assignment of each parameter to a given independent variable.

Model	A_1	A_2	A_3	A_4	A_5	A_6	A_7	A_8	R^2
CPF-1	16.4	0.5	27.4	−140.5	112.4	−0.6	−1.9	3	0.97
CPF-2	−1.9	−0.8	−2.0	4.2	−2.0	1.5	0.2	−0.3	0.73
DMT-1	26.6	48.7	−146.1	404.0	−307.1	−1.3	−1.7	18.5	0.93
DMT-2	−99.6	40.4	−137.3	422.0	−329.6	37.4	8.6	1.8	0.9999
MLT-1	431.9	−62.0	−485.7	2202.0	−1726.5	−47.4	−6.6	30.6	0.68
MLT-2	−82.6	57.7	−234.0	765.7	−563.9	25.1	0.3	−7.5	0.99

References

1. Kwong, T.C. Organophosphate pesticides: Biochemistry and clinical toxicology. *Ther. Drug Monit.* **2002**, *24*, 144–149. [CrossRef]
2. Lazarević-Pašti, T. *Organophosphates: Detection, Exposure and Occurrence*; Impact on Health and the Natural Environment; Nova Science Publishers: New York, NY, USA, 2022; Volume 1.
3. Miodovnik, A. Prenatal Exposure to Industrial Chemicals and Pesticides and Effects on Neurodevelopment. In *Encyclopedia of Environmental Health*; Nriagu, J., Ed.; Elsevier: Oxford, UK, 2019; pp. 342–352.
4. Lazarević-Pašti, T.; Anićijević, V.; Baljozović, M.; Anićijević, D.V.; Gutić, S.; Vasić, V.; Skorodumova, N.V.; Pašti, I.A. The impact of the structure of graphene-based materials on the removal of organophosphorus pesticides from water. *Environ. Sci. Nano* **2018**, *5*, 1482–1494. [CrossRef]
5. Lazarević-Pašti, T.D.; Pašti, I.A.; Jokić, B.; Babić, B.M.; Vasić, V.M. Heteroatom-doped mesoporous carbons as efficient adsorbents for removal of dimethoate and omethoate from water. *RSC Adv.* **2016**, *6*, 62128–62139. [CrossRef]
6. Anicijevic, V.; Lazarević-Pašti, T.; Vasic Anicijevic, D.; Karkalic, R. Esters of Organophosphorus Acids—Toxicity, Application and Removal from the Environment. *Sci. Tech. Rev.* **2019**, *69*, 15–29. [CrossRef]
7. Hamad, H.N.; Idrus, S. Recent Developments in the Application of Bio-Waste-Derived Adsorbents for the Removal of Methylene Blue from Wastewater: A Review. *Polymers* **2022**, *14*, 783. [CrossRef] [PubMed]
8. Osman, A.I.; El-Monaem, E.M.A.; Elgarahy, A.M.; Aniagor, C.O.; Hosny, M.; Farghali, M.; Rashad, E.; Ejimofor, M.I.; López-Maldonado, E.A.; Ihara, I.; et al. Methods to prepare biosorbents and magnetic sorbents for water treatment: A review. *Environ. Chem. Lett.* **2023**, *21*, 2337–2398. [CrossRef]
9. Fridman, L.I.; Lysenko, A.A. Carbon-Fiber Adsorbents. *Fibre Chem.* **2018**, *50*, 230–232. [CrossRef]
10. Anićijević, V.; Tasić, T.; Milanković, V.; Breitenbach, S.; Unterweger, C.; Fürst, C.; Bajuk-Bogdanović, D.; Pašti, I.A.; Lazarević-Pašti, T. How Well Do Our Adsorbents Actually Perform?—The Case of Dimethoate Removal Using Viscose Fiber-Derived Carbons. *Int. J. Environ. Res. Public Health* **2023**, *20*, 4553. [CrossRef]
11. Soffian, M.S.; Abdul Halim, F.Z.; Aziz, F.; Rahman, M.A.; Mohamed Amin, M.A.; Awang Chee, D.N. Carbon-based material derived from biomass waste for wastewater treatment. *Environ. Adv.* **2022**, *9*, 100259. [CrossRef]

12. Haghseresht, F.; Nouri, S.; Finnerty, J.J.; Lu, G.Q. Effects of Surface Chemistry on Aromatic Compound Adsorption from Dilute Aqueous Solutions by Activated Carbon. *J. Phys. Chem. B* **2002**, *106*, 10935–10943. [CrossRef]
13. Moreno-Castilla, C. Adsorption of organic molecules from aqueous solutions on carbon materials. *Carbon* **2004**, *42*, 83–94. [CrossRef]
14. Sabzehmeidani, M.M.; Mahnaee, S.; Ghaedi, M.; Heidari, H.; Roy, V.A.L. Carbon based materials: A review of adsorbents for inorganic and organic compounds. *Mater. Adv.* **2021**, *2*, 598–627. [CrossRef]
15. Al-Degs, Y.S.; El-Barghouthi, M.I.; El-Sheikh, A.H.; Walker, G.M. Effect of solution pH, ionic strength, and temperature on adsorption behavior of reactive dyes on activated carbon. *Dye. Pigment.* **2008**, *77*, 16–23. [CrossRef]
16. Newcombe, G.; Drikas, M.; Hayes, R. Influence of characterised natural organic material on activated carbon adsorption: II. Effect on pore volume distribution and adsorption of 2-methylisoborneol. *Water Res.* **1997**, *31*, 1065–1073. [CrossRef]
17. Dubinin, M.M. The Potential Theory of Adsorption of Gases and Vapors for Adsorbents with Energetically Nonuniform Surfaces. *Chem. Rev.* **1960**, *60*, 235–241. [CrossRef]
18. Sing, K.S.W. Physisorption of nitrogen by porous materials. *J. Porous Mater.* **1995**, *2*, 5–8. [CrossRef]
19. Li, L.; Quinlivan, P.A.; Knappe, D.R.U. Effects of activated carbon surface chemistry and pore structure on the adsorption of organic contaminants from aqueous solution. *Carbon* **2002**, *40*, 2085–2100. [CrossRef]
20. Bandosz, T.J. *Activated Carbon Surfaces in Environmental Remediation*; Elsevier: Amsterdam, The Netherlands, 2006.
21. Wang, S.; Zhu, Z.H.; Coomes, A.; Haghseresht, F.; Lu, G.Q. The physical and surface chemical characteristics of activated carbons and the adsorption of methylene blue from wastewater. *J. Colloid Interface Sci.* **2005**, *284*, 440–446. [CrossRef]
22. Yang, K.; Wu, W.; Jing, Q.; Zhu, L. Aqueous Adsorption of Aniline, Phenol, and their Substitutes by Multi-Walled Carbon Nanotubes. *Environ. Sci. Technol.* **2008**, *42*, 7931–7936. [CrossRef]
23. Yang, K.; Xing, B. Adsorption of Organic Compounds by Carbon Nanomaterials in Aqueous Phase: Polanyi Theory and Its Application. *Chem. Rev.* **2010**, *110*, 5989–6008. [CrossRef]
24. Jocić, A.; Breitenbach, S.; Bajuk-Bogdanović, D.; Pašti, I.A.; Unterweger, C.; Fürst, C.; Lazarević-Pašti, T. Viscose-Derived Activated Carbons Fibers as Highly Efficient Adsorbents for Dimethoate Removal from Water. *Molecules* **2022**, *27*, 1477. [CrossRef]
25. Caturla, F.; Molina-Sabio, M.; Rodríguez-Reinoso, F. Preparation of activated carbon by chemical activation with $ZnCl_2$. *Carbon* **1991**, *29*, 999–1007. [CrossRef]
26. Habila, M.A.; Alothman, Z.A.; Al-Tamrah, S.A.; Ghafar, A.A.; Soylak, M. Activated carbon from waste as an efficient adsorbent for malathion for detection and removal purposes. *J. Ind. Eng. Chem.* **2015**, *32*, 336–344. [CrossRef]
27. Wang, J.; Kaskel, S. KOH activation of carbon-based materials for energy storage. *J. Mater. Chem.* **2012**, *22*, 23710–23725. [CrossRef]
28. Bardestani, R.; Patience, G.S.; Kaliaguine, S. Experimental methods in chemical engineering: Specific surface area and pore size distribution measurements—BET, BJH, and DFT. *Can. J. Chem. Eng.* **2019**, *97*, 2781–2791. [CrossRef]
29. Jocić, A.; Breitenbach, S.; Pašti, I.A.; Unterweger, C.; Fürst, C.; Lazarević-Pašti, T. Viscose-derived activated carbons as adsorbents for malathion, dimethoate, and chlorpyrifos—Screening, trends, and analysis. *Environ. Sci. Pollut. Res.* **2022**, *29*, 35138–35149. [CrossRef] [PubMed]
30. Kupgan, G.; Liyana-Arachchi, T.P.; Colina, C.M. NLDFT Pore Size Distribution in Amorphous Microporous Materials. *Langmuir* **2017**, *33*, 11138–11145. [CrossRef]
31. Stewart, J.J. *Mopac2016*; Stewart Computational Chemistry: Colorado Springs, CO, USA, 2016.
32. Stewart, J.J.P. Optimization of parameters for semiempirical methods VI: More modifications to the NDDO approximations and re-optimization of parameters. *J. Mol. Model.* **2013**, *19*, 1–32. [CrossRef]
33. Kostoglou, M.; Karapantsios, T.D. Why Is the Linearized Form of Pseudo-Second Order Adsorption Kinetic Model So Successful in Fitting Batch Adsorption Experimental Data? *Colloids Interfaces* **2022**, *6*, 55. [CrossRef]
34. Derylo-Marczewska, A.; Blachnio, M.; Marczewski, A.W.; Seczkowska, M.; Tarasiuk, B. Phenoxyacid pesticide adsorption on activated carbon—Equilibrium and kinetics. *Chemosphere* **2019**, *214*, 349–360. [CrossRef]
35. Magdalena, B.; Anna, D.-M.; Malgorzata, S. Influence of Pesticide Properties on Adsorption Capacity and Rate on Activated Carbon from Aqueous Solution. In *Sorption in 2020s*; George, K., Nikolaos, L., Eds.; IntechOpen: Rijeka, Croatia, 2019; Chapter 1.
36. Marczewski, A.W.; Seczkowska, M.; Deryło-Marczewska, A.; Blachnio, M. Adsorption equilibrium and kinetics of selected phenoxyacid pesticides on activated carbon: Effect of temperature. *Adsorption* **2016**, *22*, 777–790. [CrossRef]
37. Tasić, T.; Milanković, V.; Batalović, K.; Breitenbach, S.; Unterweger, C.; Fürst, C.; Pašti, I.A.; Lazarević-Pašti, T. Application of Viscose-Based Porous Carbon Fibers in Food Processing—Malathion and Chlorpyrifos Removal. *Foods* **2023**, *12*, 2362. [CrossRef]
38. Yahia, M.S.; Elzaref, A.S.; Awad, M.B.; Tony, A.M.; Elfeky, A.S. Efficient adsorption of chlorpyrifos onto modified activated carbon by gamma irradiation; a plausible adsorption mechanism. *Z. Für Phys. Chem.* **2022**, *236*, 1–25. [CrossRef]
39. Vigneshwaran, S.; Preethi, J.; Meenakshi, S. Removal of chlorpyrifos, an insecticide using metal free heterogeneous graphitic carbon nitride (g-C_3N_4) incorporated chitosan as catalyst: Photocatalytic and adsorption studies. *Int. J. Biol. Macromol.* **2019**, *132*, 289–299. [CrossRef]
40. Bondžić, A.M.; Lazarević Pašti, T.D.; Pašti, I.A.; Bondžić, B.P.; Momčilović, M.D.; Loosen, A.; Parac-Vogt, T.N. Synergistic Effect of Sorption and Hydrolysis by NU-1000 Nanostructures for Removal and Detoxification of Chlorpyrifos. *ACS Appl. Nano Mater.* **2022**, *5*, 3312–3324. [CrossRef]
41. Ndifreke, W.E.; Pasaoglulari Aydinlik, N. KOH modified Thevetia peruviana shell activated carbon for sorption of dimethoate from aqueous solution. *J. Environ. Sci. Health Part B* **2019**, *54*, 1–13. [CrossRef]

42. Deshlahra, P.; Conway, J.; Wolf, E.E.; Schneider, W.F. Influence of Dipole–Dipole Interactions on Coverage-Dependent Adsorption: CO and NO on Pt(111). *Langmuir* **2012**, *28*, 8408–8417. [CrossRef]
43. Lim, S.; Kim, J.; Park, H.; Kwak, C.; Yang, J.; Kim, J.; Ryu, S.; Lee, J. Role of electrostatic interactions in the adsorption of dye molecules by Ti_3C_2-MXenes. *RSC Adv.* **2021**, *11*, 6201–6211. [CrossRef]
44. Katnić, Đ.B.; Porobić, S.J.; Vujčić, I.; Kojić, M.M.; Lazarević-Pašti, T.; Milanković, V.; Marinović-Cincović, M.; Živojinović, D.Z. Irradiated fig pomace pyrochar as a promising and sustainable sterilized sorbent for water pollutant removal. *Radiat. Phys. Chem.* **2024**, *214*, 111277. [CrossRef]
45. Breitenbach, S.; Lumetzberger, A.; Hobisch, M.A.; Unterweger, C.; Spirk, S.; Stifter, D.; Fürst, C.; Hassel, A.W. Supercapacitor Electrodes from Viscose-Based Activated Carbon Fibers: Significant Yield and Performance Improvement Using Diammonium Hydrogen Phosphate as Impregnating Agent. *C* **2020**, *6*, 17. [CrossRef]